Int. J. Solids Structures Vol. 29, No. 7, pp. 867–877, 1992
Printed in Great Britain.

0020–7683/92 $5.00 + .00

A PLANAR TYPE ANALYSIS OF THE ELASTIC–PLASTIC BEHAVIOUR OF CONTINUOUS FIBRE-REINFORCED METAL-MATRIX COMPOSITES UNDER LONGITUDINAL SHEARING AND COMBINED LOADING

NIELS SØRENSEN
Department of Solid Mechanics, The Technical University of Denmark, DK-2800 Lyngby, Denmark

(*Received* 22 *October* 1990; *in revised form* 21 *July* 1991)

Abstract—A general but essentially plane micro-mechanical model for the investigation of longitudinal shear or combined loading in continuous fibre-reinforced metal-matrix composites is presented. The model is based on the assumption that every cross-section perpendicular to the fibres deforms the same way. With this model shear, tension or compression in longitudinal or transverse directions or any combination of these loading types can be investigated. Numerical results are presented for the deformation of continuous fibre-reinforced metal-matrix composites in longitudinal shearing and longitudinal shearing combined with longitudinal tension. Results on the effect of the fibre concentration, when the material is loaded in transverse tension, are also presented. Details of the finite strain elastic-plastic behaviour of the continuous fibre-reinforced metals under longitudinal shear are discussed.

1. INTRODUCTION

The continuous fibre-reinforced metal-matrix composites, which typically consist of aluminium reinforced by long brittle boron fibres, is one of several advanced materials which has been developed in the last decade in order to combine the metallic ductility with the high strength of the fibres. The aim is to achieve a material possessing a high strength as well as a high toughness.

In research on the mechanical properties of continuous reinforced metal-matrix composites attention is typically focused on the behaviour of the material when loaded in the fibre direction, where the fibres have the strongest effect on the overall strength and stiffness. However loading in the plane perpendicular to the fibres or shearing along the fibre direction are also important situations that have to be clarified in order to characterize the material. Consider, for instance, a large thin-walled tube with circular cross-section, consisting of a ductile metal reinforced by long fibres of a brittle high-stiffness ceramic material, with the fibres parallel to the tube axis [see e.g. Dvorak *et al.* (1988)]. If such a tube is subjected to twisting or internal pressure the material will undergo shearing along the fibres or elongation perpendicular to the fibres.

In order to model the behaviour of the continuous reinforced material when subjected to longitudinal shear, transverse or longitudinal tension or compression, or any combination of these loads, a special cell-model analysis is developed in the present paper. In this cell model the full three-dimensional displacement fields are represented in terms of a planar type analysis. Finite strain elastic–plastic behaviour of the metal-matrix is accounted for, while the fibres are described as elastic.

Related cell-model analyses have been used by Christman *et al.* (1989), and Tvergaard (1990) in detailed studies of the properties of whisker reinforced aluminium. The short fibre-reinforced metal-matrix composites have some similarity with continuous reinforced metals, but the former has the disadvantage of producing large stress concentrations around the edges of the whiskers, which will eventually lead to void nucleation, as described by Nutt and Needleman (1987).

A different method has been used by Teply and Dvorak (1988), who apply the minimum principles of plasticity as the basis of their analysis to predict approximate overall properties

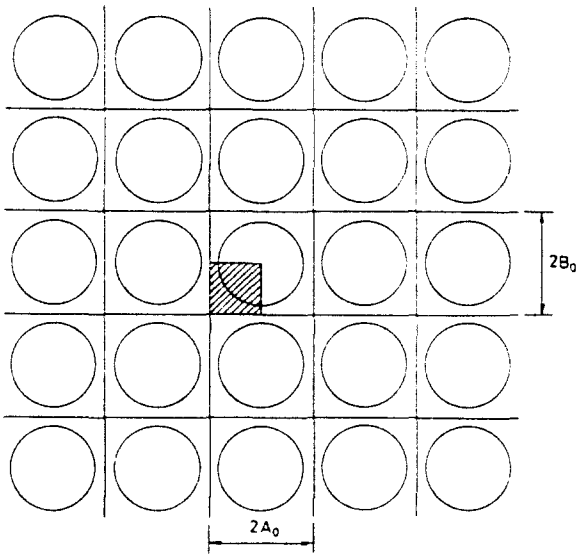

Fig. 1. Cross-section perpendicular to the continuous fibres.

of Aluminium Boron composites. Recent investigations of Brockenbrough *et al.* (1990) and Brockenbrough and Suresh (1990) use cell-model analyses to study the geometrical effects of fibre distribution and shape on the deformation of continuous fibre-reinforced metal-matrix composites.

A thorough experimental study of the properties of Aluminium Boron composites by Dvorak *et al.* (1988) suggests debonding along the interface between the fibre and the matrix as one possible mechanism that contributes to the final material behaviour. The present model does not account for debonding, but assumes perfect bonding at the interface between the matrix and the fibres [as in Christman *et al.* (1989); Tvergaard (1990); Teply and Dvorak (1988)].

2. PROBLEM FORMULATION

The cross-section perpendicular to the continuous fibres (Fig. 1), shows a regular array of fibres, with the spacings A_0 and B_0 in the initial configuration, and the fibre radius r_f. In comparison with the micrograph of a cross-section in an Aluminium Boron composite shown in Dvorak *et al.* (1988) the assumption of a periodic distribution of fibres over the cross-section is a pretty good approximation to the real material. This distribution makes the hatched area a representative unit cell, when shear, tension or compression in longitudinal or transverse directions or any combination of these loads are considered (i.e. longitudinal shearing combined with plane and axial deformation).

Figure 2 shows the deformed unit cell at two different stages of shear deformation, achieved through a constant displacement U_{III} of the upper edge of the unit cell in the x^3

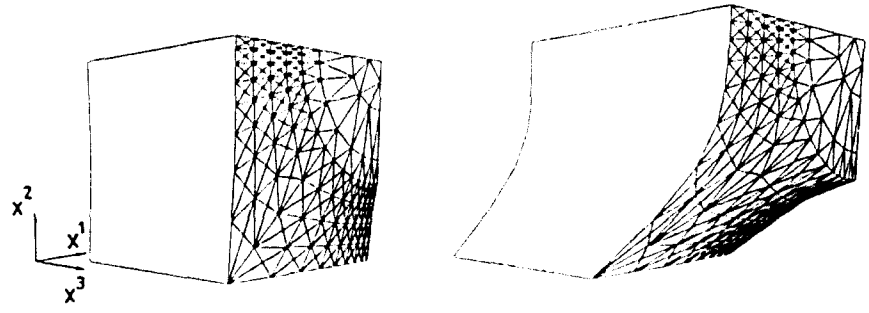

Fig. 2. Deformed unit cell at two different stages of shear deformation, achieved through displacement of the upper edge in the x^3 direction (perspective drawing).

direction. The upper edge of the unit cell is prescribed to remain straight, since this follows from the periodicity conditions. The average measure of the degree of shear deformation used here is the quantity γ defined by

$$\gamma = U_{III}/B \tag{1}$$

where B is the current dimension of the unit cell in the x^2-direction (corresponding to the initial dimension B_0). A Cartesian coordinate system x^i is used as reference, with x^1 and x^2 being coordinate directions in the cross-section perpendicular to the fibre and x^3 following the fibre direction. Figure 2 shows directly the deformed finite element net and is thus an example of the output of the model presented here. Only the deformations of the unit cell are shown in Fig. 2, but it is noted that the corresponding deformations of the full cross-section (Fig. 1) are antisymmetric about the planes $x^2 = 0$ and $x^2 = B_0$, while the deformations are symmetric about $x^1 = 0$ and $x^1 = A_0$. The fibre volume fraction f for the model material illustrated in Figs 1 and 2 is

$$f = \pi r_f^2/4A_0B_0. \tag{2}$$

The initial dimension C_0 of the unit cell along the fibre direction used for convenience in the problem formulation is the distance between two arbitrarily chosen cross-sections (Fig. 3). The current dimensions of the unit cell are denoted A, B and C and the contravariant displacement components on the reference base vectors are denoted u^i.

When sheared along the fibre direction, the material will deform in all three coordinate directions, but with the restriction that every cross-section parallel to the one shown in Fig. 1 must deform in the same way. This is the situation illustrated schematically in Fig. 3, where it is seen that the displacement gradients must be subjected to the following boundary conditions in the x^3-direction:

$$\begin{aligned} u^1_{,3} &= 0, && \text{for every } x^3 \\ u^2_{,3} &= 0, && \text{for every } x^3 \\ u^3_{,3} &= \Delta C/C_0, && \text{for every } x^3. \end{aligned} \tag{3}$$

Here the comma denotes covariant differentiation in the initial configuration of the material, while ΔC is the difference between the current length C and the initial length C_0 of the unit cell in the fibre direction.

The boundary conditions for the shear problem are

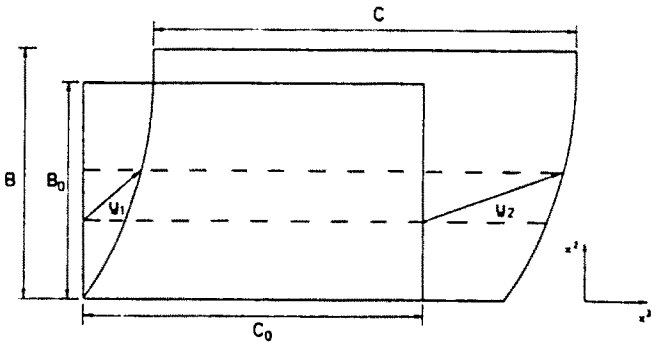

Fig. 3. Cross-section perpendicular to the x^1 direction. The deformation is restricted so that every cross-section perpendicular to the fibres must deform in the same way. From displacement vectors $\underline{u}_1$ and $\underline{u}_2$ having the same x^1 and x^2 coordinates the boundary conditions for the displacement gradients are found.

$$\begin{array}{llll} \dot{u}^1 = 0, & \dot{T}^2 = \dot{T}^3 = 0, & & x^1 = 0 \\ \dot{u}^1 = \dot{A}, & \dot{T}^2 = \dot{T}^3 = 0, & & x^1 = A_0 \\ \dot{u}^2 = 0, & \dot{T}^1 = 0, & \dot{u}^3 = 0, & x^2 = 0 \\ \dot{u}^2 = \dot{B}, & \dot{T}^1 = 0, & \dot{u}^3 = \dot{C}_{III}, & x^2 = B_0 \\ \dot{u}^1_{,3} = 0, & \dot{u}^2_{,3} = 0, & \dot{u}^3_{,3} = \dot{C}\ C_0, & x^3 = 0 \end{array} \tag{4}$$

where T^i are the components of the nominal surface tractions. (The dot means the incremental quantity.) The values of the constants $\dot{A}$, $\dot{B}$ and $\dot{C}$ are determined so that equilibrium is satisfied as described in (13).

Instead of prescribing the shear stress increment it is chosen in the present cell model to consider problems with a prescribed increment in the displacement of the upper edge of the unit cell, as specified by (4). Conditions of longitudinal shear are often specified such that $\dot{A} = \dot{C} = 0$. This is one of the possibilities included in (4), and this may lead to non-zero values of the average tractions S_1 and S_3 [see (13)]. In the computations to be presented here it is preferred to consider shear with the values of these overall tractions prescribed.

The elastic–plastic deformations of the matrix material are taken to be described by classical J_2 flow theory with isotropic hardening. In the analysis of SiC Whisker reinforced Aluminium by Christman *et al.* (1989) an elastic–viscoplastic J_2 flow theory has been used, but due to an expected small strain rate sensitivity of Aluminium, time independent plasticity theory is used here.

The finite strain generalization of J_2 flow theory used here has been discussed by Hutchinson (1973) and applied in several previous analyses [see e.g. Needleman and Tvergaard (1977) or Tvergaard (1982)]. A convected coordinate Lagrangian formulation of the field equations is used, in which g_{ij} and G_{ij} are metric tensors in the initial and current configurations respectively, with determinants g and G, and $\eta_{ij} = \frac{1}{2}(G_{ij} - g_{ij})$ are the covariant components of the Lagrangian strain tensor. The contravariant components of the Kirchhoff stress tensor are related to the components of the Cauchy stress tensor through

$$\tau^{ij} = \sqrt{\frac{G}{g}}\,\sigma^{ij}. \tag{5}$$

The incremental stress strain relation is $\dot{\tau}^{ij} = L^{ijkl}\dot{\eta}_{kl}$, where L^{ijkl} are the instantaneous moduli of J_2-flow theory, given by

$$L^{ijkl} = \frac{E}{1+\nu}\left[\tfrac{1}{2}(G^{ki}G^{jl} + G^{jl}G^{ik}) + \frac{\nu}{1-2\nu}G^{ij}G^{kl} - \alpha\frac{9(E-E_t)}{2(3E+(2\nu-1)E_t)\sigma_e^2}s^{ij}s^{kl}\right] - \tfrac{1}{2}[G^{ik}\tau^{jl} + G^{jk}\tau^{il} + G^{il}\tau^{jk} + G^{jl}\tau^{ik}]. \tag{6}$$

Here E is Young's modulus, ν is the Poisson ratio and E_t is the tangent modulus for the true stress–logarithmic strain curve. The plasticity parameter, α, is given by

$$\alpha = \begin{cases} 0, & J_2 < (J_2)_{\max} \quad \text{or} \quad \dot{J}_2 < 0 \\ 1, & J_2 \geqslant (J_2)_{\max} \quad \text{and} \quad \dot{J}_2 \geqslant 0 \end{cases} \tag{7}$$

where $(J_2)_{\max}$ is the maximum value of the J_2-invariant achieved during the loading history until the current step. The Kirchhoff stress deviator is

$$s^{ij} = \tau^{ij} - \tfrac{1}{2}G^{ij}G_{kl}\tau^{kl} \tag{8}$$

and the von Mises stress σ_e used in the J_2 flow theory, is given by

$$\sigma_e = \sqrt{\tfrac{3}{2}s_{ij}s^{ij}}\,(=\sqrt{3J_2}). \tag{9}$$

The material is chosen to follow a simple power hardening law of the form

$$\varepsilon = \begin{cases} \dfrac{\sigma_e}{E}, & \sigma_e \leqslant \sigma_y \\ \dfrac{1}{E\sigma_y^{n-1}}\sigma_e^n, & \sigma_e > \sigma_y \end{cases} \tag{10}$$

where ε is the total true strain. The strain hardening exponent is n, and the initial yield stress is σ_y.

The fibres are modelled as elastic and the instantaneous moduli in the fibres are taken to be given by an expression analogous to (6), with Young's modulus and Poisson's ratio specified by values E_f and ν_f and with no plastic deformation of the fibres ($\alpha = 0$).

3. METHOD OF ANALYSIS

The numerical incremental solution of the model problem is based on a Lagrangian formulation of the field equations. In terms of the covariant displacement components u_i on the base vectors of the Cartesian reference coordinate system the covariant components of the Lagrangian strain tensor are given by

$$\eta_{ij} = \tfrac{1}{2}(u_{i,j} + u_{j,i} + u_{,i}^k u_{k,j}). \tag{11}$$

The incremental form of the equilibrium equations used here is the incremental principle of virtual work

$$\int_V (\tau^{ij}\delta\eta_{ij} + \tau^{ij}u_{,i}^k\delta u_{k,j})\,\mathrm{d}V = \int_S \dot{T}^i\delta u_i\,\mathrm{d}S - \left[\int_V \tau^{ij}\delta\eta_{ij}\,\mathrm{d}V - \int_S T^i\delta u_i\,\mathrm{d}S\right] \tag{12}$$

where V and S are the volume and surface, respectively, of the body in the reference configuration, and the terms bracketed in (12) are included to prevent drifting of the solution from the equilibrium path [see e.g. Tvergaard (1984)]. Approximate solutions of (12) are obtained by using a finite element approximation of the displacement fields.

The deformations to be considered here can be divided into two types; one type is the deformations which are described by the deformation of the cross-section, and the other type is the deformations which make the unit cell change its length in the fibre direction, assuming that all cross-sections deform the same way (as shown in Fig. 3).

The first type of deformation can be described in the finite element model by an element with only planar interpolation functions, i.e. interpolation functions depending solely on the x^1 and x^2 coordinates (see Fig. 1), while the second type of deformation requires only a simple constant interpolation function, which is determined by the displacement gradient $u_{,3}^3$, according to eqn (3).

The element used in the model for shear and for shear combined with elongation is a simple three node triangular element, having 10 degrees of freedom. The three displacement components on the cross-section are represented by the first nine degrees of freedom with linear interpolation functions, and the last degree of freedom describes the elongation in the fibre direction.

The displacement increments related to the 10th degree of freedom in every element (describing the elongation) have the same value for all elements. Thus only one row in the global stiffness matrix is related to the 10th degree of freedom for all elements. This means that the band width of the global stiffness matrix will be quite large, but using a skyline solver, and making the column with the high skyline the last one, the computational effort is reduced. It is noted that when investigating the loading of the material perpendicular to

the fibres, conditions of plane strain are met, and then only six degrees of freedom are used per element.

The approach described here using an essentially plane model in the description of the shear behaviour of this composite material provides much lower computational costs than a full three-dimensional solution of the same problem. Yet very complex loadings, such as shearing along the fiber direction combined with axial and transverse tension or compression, can be studied with this model.

The boundary conditions (4) are implemented by a special Rayleigh-Ritz finite element method due to Tvergaard (1976), in which the special parameters chosen as unknowns are the displacement increments $\dot{A}$, $\dot{B}$ and $\dot{C}$ of the nodes on the sides of the unit cell and the value $\dot{U}_{III}$ of the increment in the displacement of the upper edge of the unit cell [see (4)]. In the solution of the linear algebraic equations for these parameters the value $\dot{U}_{III}$ is taken to be prescribed, and the unknown increments $\dot{A}$, $\dot{B}$ and $\dot{C}$ are determined so that the average true stresses normal to the surfaces of the unit cell are all equal to prescribed values S_1, S_2 and S_3. The average tractions normal to the three types of cell surfaces are

$$\begin{aligned}\langle T^1\rangle &= [\langle\sigma^1\rangle BC/(B_0C_0)] = S_1\\ \langle T^2\rangle &= [\langle\sigma^2\rangle AC/(A_0C_0)] = S_2\\ \langle T^3\rangle &= [\langle\sigma^3\rangle AB/(A_0B_0)] = S_3.\end{aligned} \tag{13}$$

Here $\langle\sigma^1\rangle$, $\langle\sigma^2\rangle$ and $\langle\sigma^3\rangle$ are the average true normal stresses on the surfaces of the unit cell. (The average stress $\langle\sigma^1\rangle$ is the stress on the cell surface with the side B and C, which is perpendicular to the x^1-direction. The average stress $\langle\sigma^2\rangle$ is the stress on the cell surface with the sides A and C, perpendicular to the x^1-direction and $\langle\sigma^3\rangle$ is the stress on the surface with the sides A and B, perpendicular to the x^3-direction of the unit cell in the initial configuration.)

4. RESULTS

4.1. *Shearing by displacement of the upper edge of the unit cell*

The results of shearing the unit cell through a constant tangential displacement U_{III} of the upper edge, while the average true normal stresses on the sides of the unit cell are all 0, are presented in Fig. 4, where the average shear stress, $\langle\tau\rangle$, on the upper side of the unit cell ($x^2 = B_0$), is shown as a function of the shear measure, γ, defined in (1) (in Fig. 4 $\langle\tau\rangle$

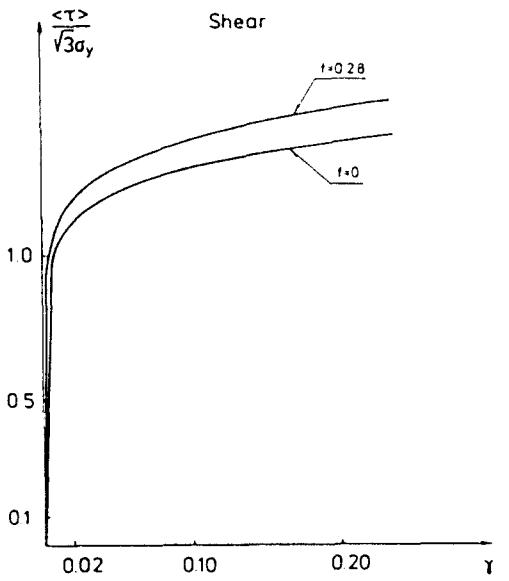

Fig. 4. The average shear stress divided by $\sqrt{3}\sigma_y$ as a function of γ ($f = 0.28$).

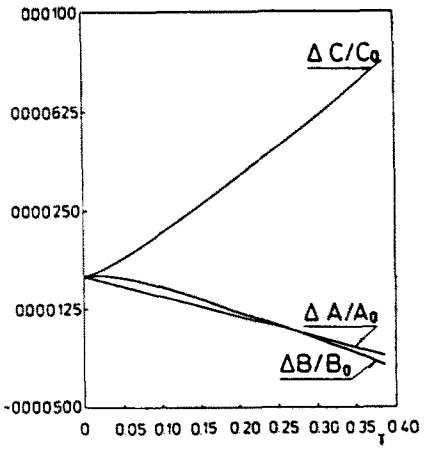

Fig. 5. The changes in the relative side lengths of the unit cell as a function of γ.

is divided by the quantity $\sqrt{3}\sigma_y$). The boundary conditions are implemented by the Rayleigh–Ritz finite element procedure, with the prescribed values $S_1 = S_2 = S_3 = 0$ [see (13)].

In the analysis of shear deformations a fibre volume fraction of $f = 0.28$ was used. The strengthening effect is not overwhelming at this concentration. Thus the shear stress $\langle\tau\rangle$ is only 8% greater than the shear stress in the material with no fibres at a value of $\gamma = 0.4$. The material parameters employed for the present study are $n = 10$, $\sigma_y/E = 0.004$, $E = 72.4$ GPa, $\nu = 0.33$ for the matrix material, and the elastic constants of the fibres are taken to be specified by $E_f/E = 5.71$ and $\nu_f = 0.21$. These values do not represent a particular material, but are chosen for convenience.

During the shear deformation of the unit cell the dimensions A, B and C increase by amounts denoted by ΔA, ΔB and ΔC, respectively, as shown in Fig. 5. When attention is focused on the change in the length of the side B it is seen that in the beginning ΔB is positive, corresponding to an increase in the height of the unit cell. Further displacement of the upper edge of the unit cell leads to a change in this behaviour when a greater part of the cross-section has become plastic. Thus the height B is decreasing, when γ becomes greater than 0.015 and after a deformation of γ greater than 0.05, ΔB is actually negative, corresponding to a lower height of the unit cell compared to the initial value B_0.

The other dimensions of the unit cell also change. Thus the length, C, in the fibre direction is increasing while the length A is reduced, corresponding to a contraction of the material in the x^1-direction.

Looking at the deformations of the unit cell at the overall deformation $\gamma = 0.2$, shown in Fig. 6a, one finds that the deformations near the top ($x^2 \simeq B$) are small, while the

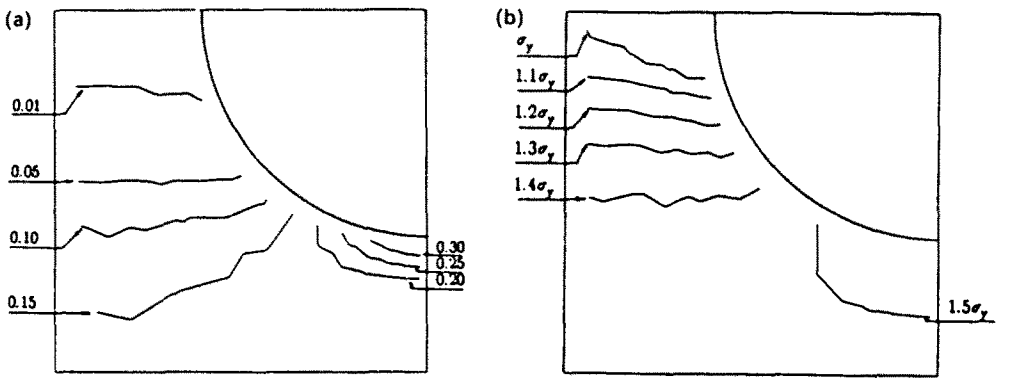

Fig. 6. Contours of constant von Mises stresses and corresponding strain contours for a shear deformed material at $\gamma = 0.20$ ($f = 0.28$).

deformations at the bottom of the unit cell are quite large. Especially the maximum deformation is achieved just below the fibre along the side $x^1 = A$. The measure of effective strain used here is simply that obtained from the uniaxial stress–strain law (10), when the current value of the von Mises stress is substituted. Shown in Fig. 6b are the corresponding levels of the von Mises stresses.

Shearing the composite to the overall deformation, $\gamma = 0.65$, does not create any unloading zones in the material with this volume concentration ($f = 0.28$), in contrast to the plane strain situation created by transverse tension are described later. As shown in Fig. 7a–b, the effective strains and the von Mises stresses are quite large in some areas in the material, at the level $\gamma = 0.65$, and it is likely that debonding will occur in the part of the unit cell just below the fibre, close to the side $x^1 = A$. This would mainly depend on the direction and the size of the shear and normal stresses along the interface as described by Needleman (1990) or Tvergaard (1989).

The results discussed here are shown in Fig. 2, where the deformed unit cell is shown at $\gamma = 0.05$ and in a perspective drawing. Especially the large local strains obtained in the area just below the fibre can be recognized in Fig. 2, at $\gamma = 0.65$.

It is noted that the shear results have great similarity with what would be found as a result of twisting a thin-walled cylindrical tube made of this material, having the fibres lying in the direction of the cylinder axis, as in the tube shown by Dvorak *et al.* (1988).

4.2. *Combined tension and shear*

Combined loading of the material in shear and axial tension has been obtained by displacement of the upper edge of the unit cell and prescribing displcements $\dot{C}$, so that the average true stress, $\langle \sigma_1 \rangle$, in the fibre direction is equal to one third of the average shear stress, $\langle \tau \rangle$, at the upper surface of the unit cell. Thus

$$\langle \sigma_1 \rangle = \frac{\langle \tau \rangle}{3}. \tag{14}$$

The problem of determining the increments in the displacements of the upper edge and the sides so that eqn (14) is satisfied and the average true normal stresses on the remaining surfaces are both zero, can again be solved using Tvergaard's method [see Tvergaard (1976)].

The average shear stress at the upper surface of the unit cell is shown in Fig. 8 as a function of the shear measure γ. Again fibre volume fractions of $f = 0.28$ and $f = 0$ was used. In Fig. 9 the change in the side lengths are shown as functions of γ, and it can be noticed that no increase in the height of the unit cell, B, is seen in this case. It is further

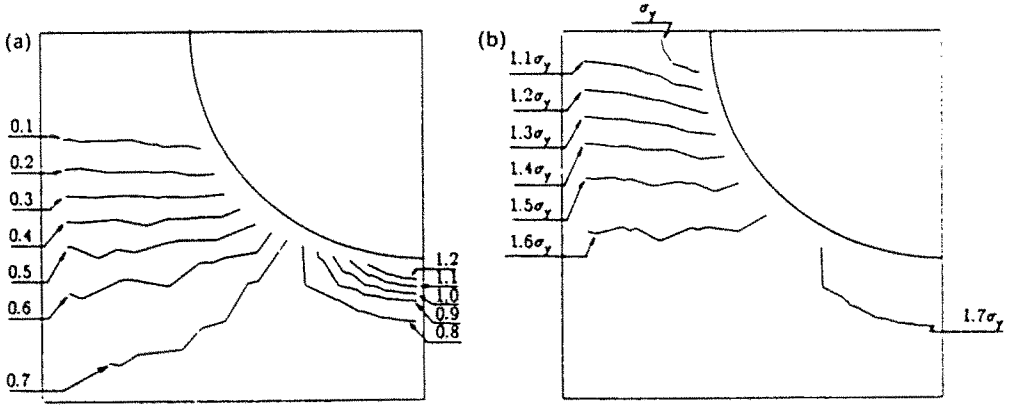

Fig. 7. Contours of constant von Mises stresses and corresponding strain contours for a shear deformed material at $\gamma = 0.65$ ($f = 0.28$).

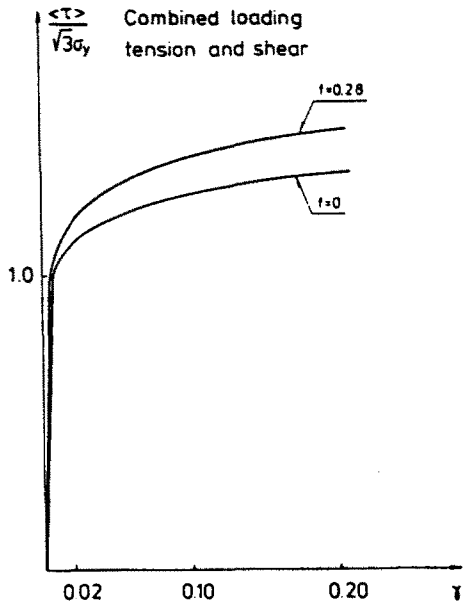

Fig. 8. Combined loading. The average shear stress divided by $\sqrt{3}\sigma_y$ as a function of γ. The normal stress (not shown) in the fibre direction is one third of the average shear stress ($f = 0.28$).

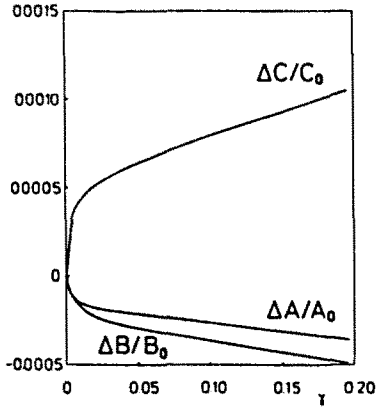

Fig. 9. The change in the relative length of the side length of the unit cell as a function of γ.

seen that only a little increase in the length in the fibre direction is achieved, corresponding to the great stiffness of the material in this direction due to the reinforcement.

The results obtained here may also be compared with the behaviour of a thin-walled tube made of this material. Then the present loading situation corresponds to combined twisting and axial tension in a metal tube reinforced by long continuous fibres in the axial direction.

4.3. *Plane deformation perpendicular to the fibre direction*

The behaviour of the fibre composite when exposed to plane deformation perpendicular to the fibre direction may also be studied in the context of the general model for the investigation of shear deformation proposed here. However, in the plane strain computations advantage is taken of the fact, that only six degrees of freedom are needed for each triangular element.

The linear strain, e_{II}, and dimensionless normal nominal stress, S_{II}, at the upper surface of the unit cell ($x^2 = B_0$) are used as overall measures for comparison of materials with different fibre concentrations. These quantities are defined by

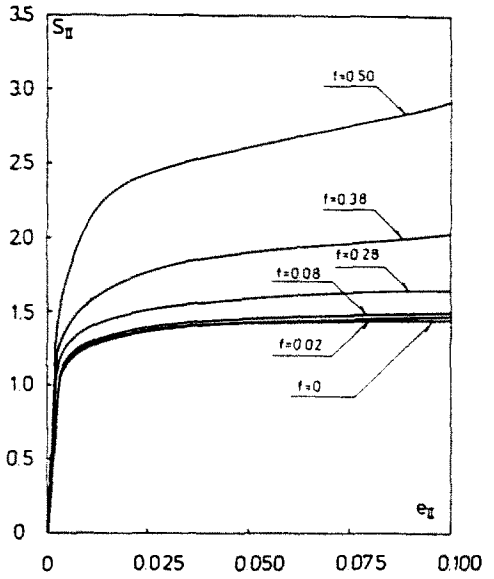

Fig. 10. Loading perpendicular to the fibre direction. Engineering stress–strain curves for different volume fractions of the continuous fibres.

$$e_{II} = \Delta B/B_0 \quad \text{and} \quad S_{II} = \langle T^2 \rangle/\sigma_y. \tag{15}$$

Shown in Fig. 10 are stress-strain curves for materials with different volume fractions of fibres. It is seen that only little influence on the overall behaviour is found when the fibre volume fractions are less than 10% ($f < 0.1$). In the material with $f = 0.28$ the overall stress is about 12% higher than that in the pure matrix material, of an overall strain $e_{II} = 0.1$. A general trend in the behaviour of the materials is that when the volume fraction is higher than $f = 0.28$ the strengthening effect increases fast with an increasing concentration, which must be a result of increasing interaction between neighbouring fibres.

Unloading also occurs in the composite, for example in the material with $f = 0.28$ when the overall strain is 0.085. For $f = 0.50$ unloading is seen already at overall strains of 0.015. It appears that this is a result of significant stress redistributions associated with strongly non-linear matrix behaviour and strong interaction with elastic fibre deformations at high values of f.

Quite large concentrations of effective strains are found near the fibre, and mechanisms such as debonding can be expected to influence the behaviour, depending on the directions of the current stresses.

In relation to the tube made of a continuous fibre reinforced metal, the analysis of a composite under transverse tension in the present section may be seen as representing a tube under internal pressure.

5. CONCLUSION

Clearly, fibres give strong improvements of the tensile properties in the direction parallel with the fibres.

The present model gives an accurate tool for analyzing the effect of continuous fibres on other types of loadings, without having to go into a full three-dimensional analysis.

It is found for shear loading that the strengthening effect is much smaller than in the axial tension loading, but when sheared to large values of γ large stresses near the interface between the matrix and the fibre are the result.

For transverse tension it is found that the strengthening effect is very small (less than 4% at $e_{II} < 0.1$) for composites with a volume fraction of fibres less than 0.1, but in composites with $f = 0.28$ or $f = 0.50$ a considerably strengthening effect is seen when the

material is deformed. Analogous effects of the reinforcement concentrations are found in a recent work in particle reinforced ductile materials by Bao *et al.* (1990).

Acknowledgement—Prof. Viggo Tvergaard of the Technical University of Denmark for useful discussions and advice during the work.

REFERENCES

Bao, G., Hutchinson, J. W. and McMeeking, R. M. (1990). Particle reinforcement of ductile matrices against plastic flow and creep. *Acta Metall. Mater.* **39**, 1871–1882.

Brockenbrough, J. R. and Suresh, S. (1990). Plastic deformation of continuous fiber-reinforced metal-matrix composites: effects of fiber shape end distribution. *Scripta Metall. et Mater.* **24**, 325–330.

Brockenbrough, J. R., Suresh, S. and Wienecke, H. A. (1990). Deformation of metal-matrix composites with continuous fibres: geometrical effects of fiber distribution and shape. Brown University Report No. NSF-DMR-8714665 MRG 4.90.

Christman, T., Suresh, S. and Needleman, A. (1989). An experimental and numerical study of deformation in metal-ceramic composites. *Acta Metall.* **37**, 3029–3050.

Dvorak, G. J., Bahei-El-Din, Y. A., Machreret, Y. and Liu, C. H. (1988). An experimental study of elastic–plastic behavior of a fibrous boron–aluminum composite. *J. Mech. Phys. Solids* **36**(6), 655–687.

Hutchinson, J. W. (1973). Finite strain analysis of elastic–plastic solids and structures. In *Numerical Solution of Nonlinear Structural Problems* (Edited by R. F. Hartung), pp. 17–29. ASME, New York.

Needleman, A. (1990). An analysis of tensile decohesion along an interface. *J. Mech. Phys. Solids* **38**, 289–324.

Needleman, A. and Tvergaard, V. (1977). Necking of biaxially stretched elastic–plastic circular plates. *J. Mech. Phys. Solids* **25**, 159–183.

Nutt, S. R. and Needleman, A. (1987). *Scripta Metall.* **21**, 705–710.

Teply, J. L. and Dvorak, G. J. (1988). Bounds on overall instantaneous properties of elastic–plastic composites. *J. Mech. Phys. Solids* **36**, 29–58.

Tvergaard, V. (1976). Effect of thickness inhomogeneities in elastic–plastic spherical shells. *J. Mech. Phys. Solids* **24**, 291–304.

Tvergaard, V. (1982). On localization in ductile materials containing spherical voids. *Int. J. Fracture* **18**, 237–252.

Tvergaard, V. (1984). Constitutive relations for creep in polycrystals with grain boundary cavitation. *Acta Metall.* **32**, 1977–1990.

Tvergaard, V. (1989). Effect of fibre debonding in a whisker-reinforced metal. DCAMM Report No. 400, The Technical University of Denmark.

Tvergaard, V. (1990). Analysis of tensile properties for a whisker-reinforced metal–matrix composite. *Acta Metall. Mater.* **38**, 185–194.